Available online at www.sciencedirect.com
SCIENCE DIRECT®
Journal of Power Sources 119–121 (2003) 815–820
JOURNAL OF POWER SOURCES
www.elsevier.com/locate/jpowsour

# MRSST a new method to evaluate thermal stability of electrolytes for lithium ion batteries

Gerardine G. Botte*, Timothy J. Bauer

*Department of Chemical Engineering, University of Minnesota Duluth, 207 Engineering Building, Duluth, MN 55812, USA*

**Abstract**

The use of the Modified Reactive System Screening Tool (MRSST) to study the thermal stability of electrolytes for lithium ion batteries was demonstrated. Important data for the understanding of the thermal behavior of lithium ion batteries (vapor liquid equilibrium data, heat capacity, heats of vaporization, reaction rates, and heats of reaction) can be obtained with the MRSST. The technique also allows sampling of the system (gas phase or liquid phase) at any time. The thermal stability of EMC and EC was analyzed using the MRSST. The results indicated that EMC is thermally stable until 320 °C, while the EC decomposes at 263 °C generating gases such as $CO_2$, $O_2$, and $H_2$. The effect of $O_2$ on the thermal stability of EMC was also studied. It was found that EMC thermally decomposes in the presence of $O_2$ between 220 and 235 °C generating non-condensable gases such as $CO_2$.


*Keywords:* Modified Reactive System Screening Tool; Thermal stability; Electrolyte decomposition; Thermal runaway; Gas evolution

## 1. Introduction

In order to understand the safety concerns (thermal runaway) associated with lithium ion batteries, some researchers [1–20] have performed thermal stability studies on these batteries. The most common experimental techniques that have been used in the thermal studies are differential scanning calorimetry (DSC) and adiabatic calorimetry (ARC). These techniques are good for preliminary evaluation of thermal stability; they can be used to obtain important information such as: heats of reaction, temperature of decomposition, and empirical reaction rates as a function of the extent of the reaction. However, more information is required to have a better understanding of the decomposition reactions: pressure effect, variation of concentration of reactants as a function of time, products generated, gas evolution, etc. This information cannot be obtained from a DSC because of the limitations of the technique (i.e. DSC hermetically sealed pans cannot be sampled easily). An ARC can be used to obtain pressure variations in the battery but the technique is not very flexible to perform a detailed kinetics study of the thermal decomposition reactions that can take place in the materials of the battery (i.e. sampling of the system is not easy).

The specified information can be obtained in a quickly and safely way using a Reactive System Screening Tool (RSST) [21]. The RSST is a type of calorimeter that can determine potential chemical hazards. It allows recording temperatures, and pressures of the system, and at the same time permits sampling or adding of new sample at any point during the reaction. The use of the RSST has proven itself successful in studying liquid phase reactions. However, the study of gas phase reactions in the RSST causes some problems (i.e. condensation of vapors on the containment walls inhibits the RSST from reaching the onset temperature of a gas and/or gas–liquid phase reactions). To overcome some of the problems we have designed a novel method, Modified Reactive System Screening Tool (MRSST), which allows determining thermal stability data for solvents and electrolytes used in lithium ion batteries. The MRSST keeps the same advantages of the RSST and at the same time can be used for liquid–gas phase reactions.

The objective of this paper is to describe the new method (MRSST), and to demonstrate its reliability to evaluate the thermal stability of electrolytes for lithium ion batteries. Ethyl–methyl carbonate (EMC) and ethylene carbonate (EC) were the solvents used during the study. These solvents were chosen because of their intensive use in commercial lithium ion batteries. The aim of this work is to provide a better understanding of the thermal stability of electrolyte mixtures, which is crucial in the design of safe and high-performance lithium ion batteries.

* Corresponding author. Present address: Russ College of Engineering and Technology, Ohio University, 183 Stocker Center, Athens, OH 45701, USA.
*E-mail address:* botte@bobcat.ent.ohiou.edu (G.G. Botte).

0378-7753/03/$ – see front matter © 2003 Elsevier Science B.V. All rights reserved.
doi:10.1016/S0378-7753(03)00247-7

## 2. Description of the equipment

Our design is a modification of the RSST designed by Fauske & Associates Inc. [21]. The study of gas phase reactions and/or liquid–gas phase reactions in the RSST causes some problems. We have identified some of these problems during the evaluation of the technique for the thermal analysis of solvents used in lithium ion batteries. Problems arise with the use of the RSST when vapors condense on the containment walls. This inhibits the RSST from reaching the onset temperature of the reaction. To solve the problems described above we have redesigned the original RSST for what we have called a MRSST.

Fig. 1 presents a schematic diagram of the MRSST. The MRSST consists of a high pressure containment vessel with a sample container inside, two thermocouples, and a pressure transducer. The thermocouples are directly fed through the container wall. Thermocouple 1 (T1) is used to measure the temperature of the sample, and thermocouple 2 (T2) is used to measure the containment vessel wall temperature. The sample is heated by using external heaters to heat the containment vessel. The total heat added by the heaters to the system is quantified. Heating elements are used at the top, bottom, and around the sides as to completely cover the vessel, in order to prevent any vapors from condensing inside the vessel. The sample is heated at a constant rate of 10 °C/min. The temperature of the sample is kept homo-

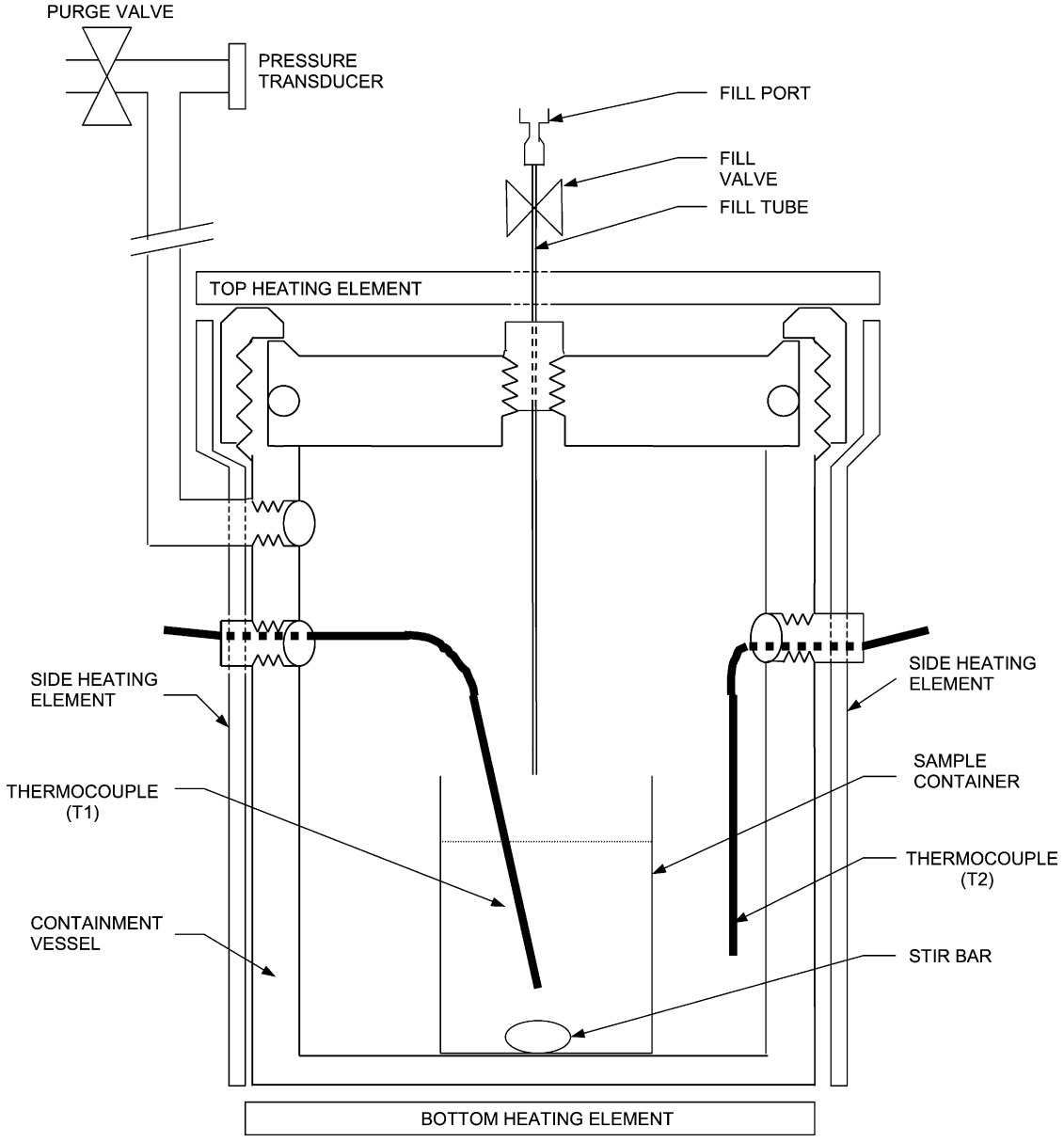


Fig. 1. Schematic diagram of Modified Reactive System Screening Tool (MRSST). The system is very flexible. The sample line allows sampling or adding of new sample at any point during the reaction, therefore detailed kinetics studies can be performed with the MRSST.

genous by mixing with a stir bar. Temperatures and pressures can be monitored all time during the process. As shown in Fig. 1, the MRSST posses a sample line that allows sampling or adding of new sample at any point during the reaction.

## 3. Modeling equations

Because of the constant heat rate, and the absence of heat losses the MRSST can be modeled as an adiabatic cell. Considering the following assumptions: (1) adiabatic reactor; (2) no thermal conductivity resistance; (3) closed system; and (4) constant volume; the energy balance during a reaction is given by

$$(\phi_{\mathrm{MRSST}} + mC_p)\frac{\mathrm{d}T}{\mathrm{d}t} = VM_{\mathrm{w}}\,\Delta H_{\mathrm{r}}\Re \tag{1}$$

where $m$ is the mass of the sample (g), $C_p$ the heat capacity of the sample (J/(g K)), $V$ the volume of the containment vessel ($m^3$), $M_{\mathrm{w}}$ the molecular weight of the limiting reactant (g/mol), $\Delta H_{\mathrm{r}}$ the heat of reaction (J/g) and $R$ the rate of the reaction (mol/($m^3$ s)). The ratio between d$T$/d$t$ is known as the self-heating rate (K/s). The factor $\phi_{\mathrm{MRSST}}$ is defined by:

$$\phi_{\mathrm{MRSST}} = m_{\mathrm{sc}}C_{p_{\mathrm{sc}}} + m_{\mathrm{v}}C_{p_{\mathrm{v}}} \tag{2}$$

where $m_{\mathrm{sc}}$ and $C_{p_{\mathrm{sc}}}$ are the mass (g) and the heat capacity (J/(g K)) of the sample container, respectively; and $m_{\mathrm{v}}$ and $C_{p_{\mathrm{sc}}}$ are the mass (g) and the heat capacity (J/(g K)) of the containment vessel, respectively.

The reaction rate is a function of the concentration and temperature and can be expressed in general form as

$$\Re = \frac{\mathrm{d}C}{\mathrm{d}t} \tag{3}$$

where d$C$/d$t$ represents the variation of the concentration of the limiting reactant as a function of time (mol/($m^3$ s)).

Substituting Eq. (3) into Eq. (1), integrating between the initial temperature ($T_{\mathrm{i}}$) and the final temperature ($T_{\mathrm{f}}$) of the reaction, and assuming that the heat capacities of the sample, sample container, and containment vessel are constant, yields

$$C = C_0\left[\frac{T_{\mathrm{f}} - T}{T_{\mathrm{f}} - T_{\mathrm{i}}}\right] \tag{4}$$

where $C_0$ is the initial concentration of the limiting reactant (mol/$m^3$). Eq. (4) can be expressed as a function of the extent of the reaction instead by

$$1 - \alpha = \left[\frac{T_{\mathrm{f}} - T}{T_{\mathrm{f}} - T_{\mathrm{i}}}\right] \tag{5}$$

The heat of the reaction can be calculated by

$$\Delta H_{\mathrm{r}} = -\frac{(\phi_{\mathrm{MRSST}} + mC_p)(T_{\mathrm{f}} - T_{\mathrm{i}})}{VM_{\mathrm{w}}C_0} \tag{6}$$

Finally, substituting Eq. (6) into Eq. (1) and using the definition of extent of the reaction:

$$\frac{\mathrm{d}T}{\mathrm{d}t} = (T_{\mathrm{f}} - T_{\mathrm{i}})\frac{\mathrm{d}\alpha}{\mathrm{d}t} \tag{7}$$

Eq. (7) allows determining reaction rates using the MRSST. It can be noticed that because of the adiabatic assumption all the equations are comparable with the equations used for measurement of reaction rates using an adiabatic calorimeter (ARC). Nevertheless, the sampling capability of the MRSST also allows obtaining reaction rates as a direct measurement of the variation of the concentration of one of the species with time.

One of the great advantages of the MRSST is that not only the temperature but also the pressure of the system is recorded simultaneously. Therefore, for vapor–liquid systems, the vapor pressure can be measured. The vapor pressure can be fitted for a wide range of temperatures using Riedel's correlation [22]:

$$P^{\mathrm{sat}} = 101,000\,\mathrm{e}^{(A-\{B/(T-273)\}+C\ln[T-273]+D[T-273]^6)} \tag{8}$$

where $P^{\mathrm{sat}}$ is the saturation pressure (Pa), and $A$ (dimensionless), $B$ (K), $C$ (dimensionless), and $D$ ($K^{-6}$) are Riedel's constants.

In addition, the heat of vaporization can be calculated by using Clapeyron equation [23]:

$$\Delta H_{\mathrm{v}} = T\,\Delta V\frac{\mathrm{d}P^{\mathrm{sat}}}{\mathrm{d}T} \tag{9}$$

where $\Delta H_{\mathrm{v}}$ is the heat of vaporization (J/mol), and $\Delta V$ the compressible volume ($m^3$/mol). The saturation pressure and the temperature should be given in Pa and K, respectively. Neglecting the volume of the liquid (much smaller than the volume of the gas) and assuming ideal gas, Eq. (9) becomes

$$\Delta H_{\mathrm{v}} = T^2\frac{R}{P^{\mathrm{sat}}}\frac{\mathrm{d}P^{\mathrm{sat}}}{\mathrm{d}T} \tag{10}$$

where $R$ is the universal gas constant (8.314 J/(mol K)). Eq. (10) is known as Clausius–Clapeyron relation [23].

Another important property that can be measured with the system is the heat capacity of the sample. For samples that go through a phase change or that have two phases in equilibrium (vapor–liquid), the heat capacity of the sample (vapor–liquid) can be calculated by:

$$C_p = \frac{V_{\mathrm{sc}}}{V}\frac{vI}{(\mathrm{d}T/\mathrm{d}t)m} - \frac{V_{\mathrm{sc}}}{V}\frac{\Delta H_{\mathrm{v}}(\mathrm{d}n/\mathrm{d}t)}{(\mathrm{d}T/\mathrm{d}t)m} - \frac{m_{\mathrm{sc}}C_{p_{\mathrm{sc}}}}{m} \tag{11}$$

where $v$ is the voltage (V) of the heaters, $I$ the current through the heaters (A), d$n$/d$t$ the evaporation rate (mol/s), and $V_{\mathrm{sc}}$ the volume of the sample container ($m^3$). The heat capacity of the sample container has been assumed constant for the derivation of Eq. (11). The first term in Eq. (11) represents the total heat that goes into the system (sample and sample container), the second term represents the heat that is used for evaporation of the sample, and the last term represents the heat that goes to the sample container. Eq. (11)

can be used to calculate the heat capacity of the sample at different temperatures, or it can be integrated over a range of temperatures to obtain an average sample heat capacity. Assuming ideal gas the evaporation rate can be calculated by:

$$\frac{dn}{dt} = \frac{V}{R}\left(\frac{1}{T}\frac{dP}{dt} - \frac{P}{T^2}\frac{dT}{dt}\right) \quad (12)$$

## 4. Experimental

The solvents EMC and EC were obtained from EM Industries Inc. All of them were 99.9% pure with less than 30 ppm of water. The samples were prepared in an Argon filled glove box. The weight of the samples was kept between 15 and 18 g. The reactor was heated at 10 °C/min from room temperature to 320 °C. The temperatures ($T1$ and $T2$) and the pressure were monitored all the time. The gases evolved from the decomposition were analyzed using gas chromatography and titration.

## 5. Results and conclusions

Fig. 2 shows the variation of the pressure of the EMC as a function of temperature. No reactions were observed for the given range of temperatures, which agrees well with the DSC results reported by Botte et al. [19]. The figure shows three distinguished areas: system equilibration, vapor–liquid equilibrium (VLE), and complete evaporation of the s ample. The vapor pressure in Pa for EMC can be fitted very well using Riedel's correlation (Eq. (8)) for a temperature range of 393–504 K with the following parameters: $A = 69.561$, $B = 9100.2$, $C = -7.789$, and $D = -2.03 \times 10^{-17}$. Determination of the temperature–pressure relations and vapor pressure of the solvents is very important to predict the pressure of lithium ion batteries. The heat of vaporization for EMC was calculated using Eq. (10). The calculated heat is $43 \pm 4$ kJ/mol. The heat of vaporization for the EMC is not reported in the literature, however, this value compares very well with the heat of vaporization reported for DEC (43.6 kJ/mol [24]) which indicates confidence in the technique.

Fig. 3 shows the effect of oxygen on the thermal stability of EMC. The figure indicates that EMC thermally decomposes in the presence of $O_2$ between 220 and 235 °C as demonstrated by the pressure peaks shown in the figure. The effect of different initial concentrations of $O_2$ was also evaluated: mixtures of EMC with 5, 10, 15, and 20 psi of $O_2$ were used. It can be noticed that the larger the $O_2$ concentration, the higher the maximum pressure of the system during the reaction, and the higher the temperature of decomposition. All the curves overlap before decomposition starts because the EMC in liquid phase is in equilibrium with the vapor phase. The fact that the decomposition temperature increases with increasing the $O_2$ concentration implies that EMC must reach a certain concentration in gas phase before it reacts with $O_2$. This indicates that by controlling the amount of EMC evaporated to a minimum value any thermal decomposition with $O_2$ can be avoided. $O_2$ is the limiting reactant for the reaction peaks shown in Fig. 3. When the reaction starts, the pressure increases indicating the formation of gases; once the reaction is over (due to the consumption of $O_2$) the pressure in the system drops because some of the EMC in the gas phase suddenly condenses (due to the higher pressure) until it reaches vapor–liquid equilibrium again. Finally, the whole system changes to gas phase due to the increase of temperature. It was observed, that the larger the initial concentration of $O_2$ in the system, the larger the amount of gases generated during the decomposition.

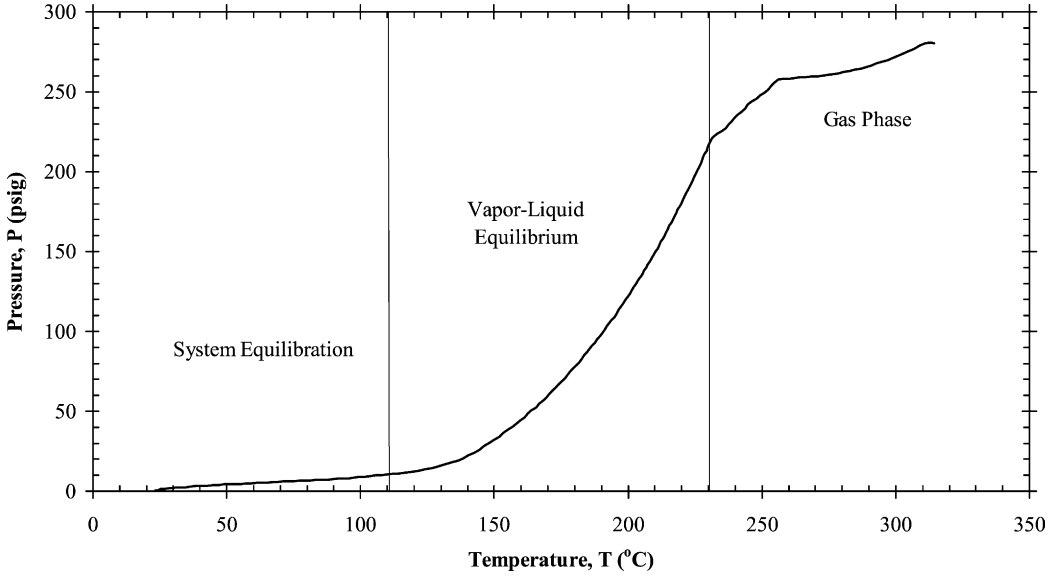


Fig. 2. Variation of the EMC pressure as a function of the temperature. The vapor pressure can be fitted using Riedel's correlation [22].

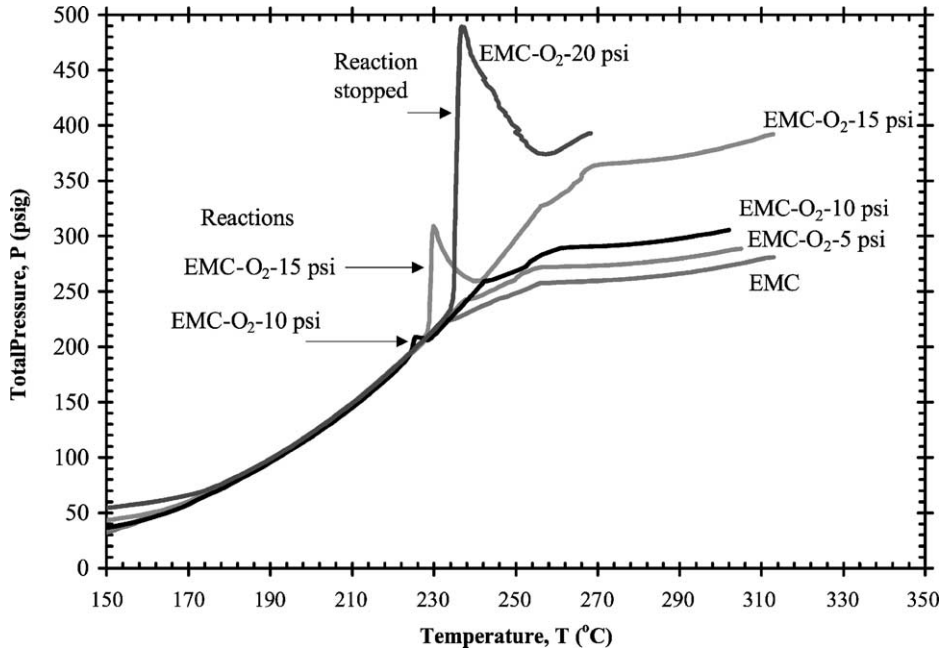


Fig. 3. Effect of oxygen on the thermal stability of EMC. The EMC reacts with $O_2$ between 220 and 235 °C. The larger the $O_2$ concentration the higher the total pressure of the system (the larger the amount of gases generated during the reaction). Thermal runway was observed for the mixture of EMC with 20 psi of $O_2$. The formation of $CO_2$ was observed during the decomposition.

A strong reaction peak is not observed for the EMC–$O_2$–5 psi mixture (due to the low concentration of $O_2$); however, thermal decomposition in this system was verified by the generation of gases. For the EMC–$O_2$–20 psi mixture, thermal runway was observed; the pressure of the system increased really fast, and almost reached 500 psi (see Fig. 3) which is the set point for breaking the rupture disk in the MRSST. The reaction was stopped externally by cooling down the MRSST.

For all the EMC–$O_2$ mixtures shown in Fig. 3, the final pressure of the system (after cooling down to initial temperature) was higher than the initial pressure, indicating the formation of non-condensable gases. The non-condensable gases were collected in water. The solution obtained was titrated with NaOH to measure the $CO_2$ concentration ($H_2CO_3$). The titration measurements revealed the formation of $CO_2$ during the decomposition. The $CO_2$ concentrations were 0.00256, and 0.00022 mol/l for the EMC–$O_2$–20 psi and the EMC–$O_2$–15 psi mixtures, respectively. The higher the initial oxygen pressure the larger the $CO_2$ concentration measured in the system. The presence of $CO_2$ indicates that a combustion reaction may be taking place as suggested by Botte et al. [19]. The average heat of reaction for the thermal decomposition of EMC in the presence of $O_2$ was calculated by using Eq. (6) with $O_2$ as the limiting reactant. The heat capacity of the system used in Eq. (6) was calculated using Eq. (11). The sample heat capacity (vapor–liquid phase) calculated was $1.7 \pm 0.4$ J/(g K), this value compares very well with the heat capacities of the ethylene carbonate and diethyl carbonate reported in the literature, 1.5 [25] and 1.7 J/(g K) [26], respectively. The difference between the final and the initial temperatures of reaction ($T_f - T_i$) depends on the total amount of $O_2$ in the system (see Fig. 3), for the mixture EMC–$O_2$–15 psi the temperature difference is 12 °C (see Fig. 3); therefore, the calculated heat of reaction is $\Delta H_r = 19{,}500 \pm 2200$ J/g. This value compares very well with the heat of reaction reported by Botte et al. [19], $\Delta H_r = 12{,}200 \pm 1200$ J/g (value calculated using the estimated amount of $O_2$ present in the DSC pan reported by the authors [19]). The calculated heat of reaction lays in the range of the heat of combustion for the EC and DEC reported in the literature: $12{,}151 \pm 24$ and 22,648 J/g, respectively [27]. This fact also supports the combustion hypothesis.

Fig. 4 shows the variation of the pressure of the EC as a function of temperature. The system is thermally stable until 263 °C, at this temperature thermal decomposition is observed (as demonstrated by the abrupt increase of pressure in the system). The final pressure of the system (after cooling down to the initial temperature) was much higher than the initial pressure, indicating the formation of non-condensable gases during the decomposition. The gases were analyzed using a gas chromatograph, $CO_2$ was the major component (15.15%), with the formation of some $O_2$ (422 ppm) and traces of $H_2$ (33 ppm). The results indicated that EC can be a source of oxygen inside the battery; therefore, the thermal decomposition of EC should be studied in detail.

In conclusion, the results obtained indicate that the MRSST is an excellent technique that can help understanding the thermal behavior of lithium ion batteries. The technique can be extended to analyze the thermal performance of electrodes and batteries.

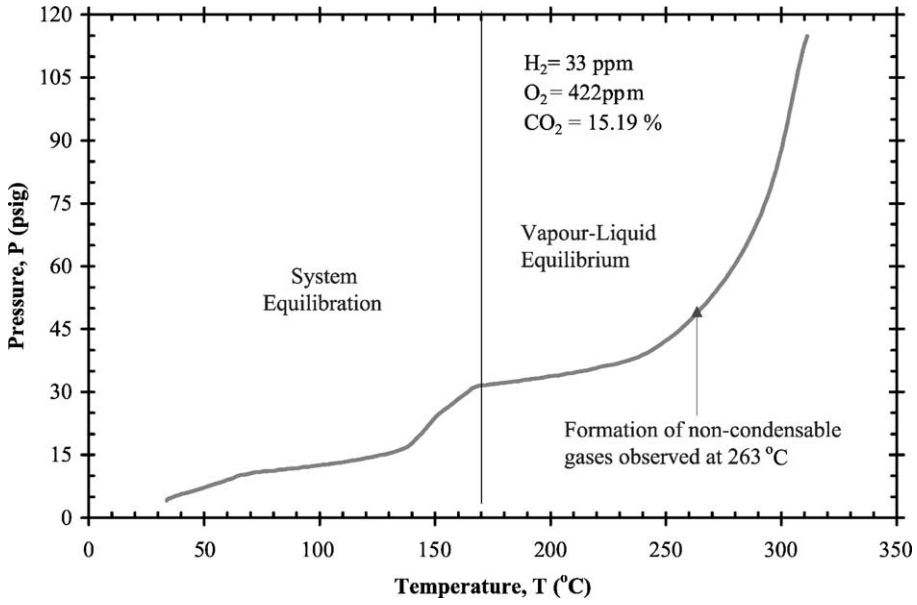


Fig. 4. Variation of the EC pressure as a function of temperature. The EC decomposed at 263 °C releasing gases such as: $H_2$, $O_2$ and $CO_2$.

## Acknowledgements

Financial support for this work was partially provided by Solvay, and the University of Minnesota Grant-in-Aid of research, artistry and scholarship.

## References

[1] Z. Zhang, D. Fouchard, J.R. Rea, J. Power Sources 70 (1998) 16.
[2] U. von Sacken, E. Nodwell, A. Sundher, J.R. Dahn, Solid State Ionics 69 (1994) 284.
[3] J.R. Dahn, E.W. Fuller, M. Obravac, U. von Sacken, Solid State Ionics 69 (1994) 265.
[4] R. Fong, U. von Scaken, J.R. Dahn, J. Electrochem. Soc. 137 (1990) 2009.
[5] A.N. Dey, B.P. Sullivan, J. Electrochem. Soc. 117 (1970) 222.
[6] M.A. Gee, F.C. Laman, J. Electrochem. Soc. 140 (1993) L53.
[7] S.I. Tobishima, K. Hayashi, K. Saito, T. Shodai, J.-I. Yamaki, Electrochim. Acta 42 (1997) 119.
[8] A. Du Pasquier, F. Disma, T. Bowmer, A.S. Gozdz, G. Amatucci, J.M. Tarascon, J. Electrochem. Soc. 145 (1998) 472.
[9] J.-S. Hong, H. Maleki, S. Al Hallaj, L. Redey, J.R. Selman, J. Electrochem. Soc. 145 (1998) 1489.
[10] M.N. Richard, J.R. Dahn, J. Electrochem. Soc. 146 (1999) 2068.
[11] M. Arakawa, J.-I. Yamaki, T. Okada, J. Electrochem. Soc. 131 (1984) 2605.
[12] M. Arakawa, J.-I. Yamaki, J. Electroanal. Chem. 219 (1987) 273.
[13] Z.X. Shu, R.S. McMillan, J.J. Murray, J. Electrochem. Soc. 140 (1993) L101.
[14] A. Ohta, H. Koshina, H. Okuno, H. Murai, J. Power Sources 54 (1995) 6.
[15] K. Takei, K. Kumai, T. Iwahori, T. Uwai, M. Furusyo, Denki Kagaku 61 (1993) 421.
[16] M. Namba, K. Ikawa, M. Mizumoto, S. Nishimura, Y. Nakamura, T. Shishikura, Denki Kagaku 59 (1991) 770.
[17] R. Imhof, P. Novak, J. Electrochem. Soc. 146 (1999) 1702.
[18] G.G. Botte, R.E. White, Z. Zhang, J. Power Sources 97–98 (2001) 570.
[19] G.G. Botte, Y. Wulandari, R.E. White, Z. Zhang, Effect of Water and Oxygen on the Thermal Stability of $LiPF_6$EC:EMC Electrolyte for Lithium Ion Batteries, The Electrochemical Society, Meeting Abstracts (099), San Francisco, CA, September 2–7, 2001.
[20] D.D. MacNeil, J.R. Dahn, J. Phys. Chem. A 105 (2001) 4430.
[21] Reactive System Screening Tool, System Manual, Fauske & Associates Inc. (http://www.fauske.com/welcome.htm), July 1994.
[22] R.H. Perry, D.W. Green, Perry's Chemical Engineering Handbook, McGraw-Hill, Singapore, 1984.
[23] J.M. Smith, H.C.V. Ness, Termodinamica en Ingenieria Quimica, McGraw-Hill, Mexico, 1980, p. 199.
[24] D.R. Lide, CRC Handbook of Chemistry and Physics, CRC Press, Florida, 1998, p. 3/111.
[25] W.J. Peppel, Ind. Eng. Chem. 50 (1958) 767.
[26] N.A. Kolosovskii, W.W. Udovenko, Zhur. Obshchei Khim 4 (1934) 1027.
[27] J.K. Choi, M.J. Joncich, J. Chem. Eng. Data 16 (1971) 87.